JOURNAL OF MATERIALS SCIENCE **39** (2004) 4877–4885

Characterization of oxygen passivated iron nanoparticles and thermal evolution to γ-Fe_2O_3

T. C. ROJAS*, J. C. SÁNCHEZ-LÓPEZ
Instituto de Ciencia de Materiales de Sevilla and Dpto. de Química Inorgánica, Centro de Investigaciones Científicas Isla de la Cartuja, Avda. Américo Vespucio s/n, 41092-Sevilla, Spain
E-mail: tcrojas@cica.es

J. M. GRENECHE
Laboratoire de Physique de l'Etat Condensé, UMR CNRS 6087, Université du Maine, 72085 Le Mans Cedex France

A. CONDE
Instituto de Ciencia de Materiales de Sevilla and Dpto. de Física de la Materia Condensada, P.O. Box 1065, 41080-Sevilla, Spain

A. FERNÁNDEZ
Instituto de Ciencia de Materiales de Sevilla and Dpto. de Química Inorgánica, Centro de Investigaciones Científicas Isla de la Cartuja, Avda. Américo Vespucio s/n, 41092-Sevilla, Spain

Nanocrystalline iron powders have been prepared by the inert gas evaporation method. After preparation the material has been passivated by pure oxygen and air exposure. In the present paper we describe new characterization studies of this sample by Transmission Electron Microscopy (TEM), X-ray Diffraction (XRD), X-ray Absorption Spectroscopy (XAS), Electron Energy Loss Spectroscopy (EELS) and Mössbauer Spectroscopy (MS), giving a complete chemical and structural characterization of the nanocomposite material in order to correlate its microstructure with its singular magnetic behavior.

This nanocomposite was later heated following different thermal treatments. It was found that the sample heated successively in high vacuum (10^{-7} torr) at 383 K for 1 h and under a residual oxygen pressure of 4×10^{-4} torr at 573 K for 3 h, results in a powder formed by nanoparticles of γ-Fe_2O_3 as stated from XRD, XAS and MS. This material is stable during several years and behaves almost totally like superparamagnetic at room temperature.

1. Introduction

The fabrication and characterization of nanosized magnetic particles are the subject of intense research motivated not only by their interesting properties, quite different from those of the corresponding bulk materials, but also from the point of view of their promising technological applications, such as magnetic recording media, ferrofluids, etc. . . .[1–4].

A number of research works have been published during the last few years dealing with the magnetic behaviour of nanometre sized Fe, Co and Ni crystalline particles synthesized by different techniques and presenting different degrees of surface oxidation [5–14]. The singular magnetic behaviour of these systems has been found to be dependent on the size and the surface characteristic of the particles, and it is attributed to the large magnetic anisotropies observed in these materials. In particular, exchange anisotropy was first discovered by Meiklejohn and Bean [11] in compacted oxide-coated Co particles. In spite of the numerous publications on the magnetic properties of oxide coated Fe, Co and Ni nanoparticles, there is still a limited number of studies with a complete characterization at the microstructural level, that allows to achieve a better understanding of their magnetic properties [12, 15–17].

In the present work, Fe nanoparticles have been prepared by the inert gas evaporation method [18]. Exposure of the sample to an oxygen atmosphere produces passivation of the particles with an amorphous oxide layer [19]. Previous data obtained by X-ray Photoelectron Spectroscopy (XPS) for the oxygen passivated Fe nanocrystalline powder have been already reported [18, 19] together with the magnetic behavior of this material [12, 20]. In the present paper new results obtained

*Author to whom all correspondence should be addressed.

by Transmission Electron Microscopy (TEM), X-ray Diffraction (XRD), X-ray Absorption Spectroscopy (XAS), Electron Energy Loss Spectroscopy (EELS), and Mössbauer Spectroscopy (MS), are discussed. In particular new data related to the microstructural characterization of the oxide layer and the magnetic behavior of the sample are reported.

In addition to that, the study of the thermal evolution of the oxygen passivated iron nanoparticles allowed us to determine a procedure for the complete transformation of this material into nanocrystalline γ-Fe_2O_3. Superparamagnetic nanoparticles of the maghemite phase have been already reported [21, 22], being the procedure presented here an alternative method for the synthesis of this material.

2. Experimental

Nanocrystalline Fe particles have been prepared by evaporation of Fe in a W boat at 1773 K [19]. The gas phase used during evaporation was He at 133 Pa (1 torr). Through interatomic collisions with the inert-gas atoms, the evaporated atoms lose kinetic energy and condense as an ultrafine powder that accumulates on a cold finger [23]. After passivation by O_2 (266 Pa for 10 min) and air exposure the material was stripped off and stored in a dessicator. This as-prepared sample was then heated under different residual vacuum pressures and temperatures as indicated in the text.

TEM examination of the samples was carried out in a Philips CM200 microscope working at 200 kV. The particles were dispersed in ethanol by sonication and dropped on a copper grid coated with a carbon film.

XRD analysis was carried out using Cu K_α radiation in a Siemens D5000 diffractometer.

XAS spectra were recorded at the DCI storage ring in LURE (France), running at 1.85 GeV with an average current of 250 mA. Monochromatization of the beam was carried out through a Si (111) double crystal monochromator. The detection of the XAS absorption coefficient was done in the transmission mode for the samples that were supported on cellulose filters. Spectra were recorded at the Fe-K edge at ca. 7120 eV. To compare the XAS spectra a linear background was fitted in the pre-edge region and subtracted before normalisation to the edge jump.

EELS spectra were acquired in the Jeol 2010 FEG microscope (Ecole Centrale de Lyon) operating at 200 kV, probe size between 0.5 and 2.4 nm, point resolution ca. 0.19 nm. It is equipped with a PEELS spectrometer (GATAN 766-2 K).

^{57}Fe Mössbauer spectra were recorded in a bath cryostat at several temperatures. In-field spectra were recorded using a cryomagnetic device where the external magnetic field is applied parallel to the γ-beam. A conventional transmission Mössbauer spectrometer, operating in the constant acceleration mode, was used. The hyperfine structure was modelled by means of distribution of lorentzian shape line quadrupolar doublets or magnetic sextets using a least square fitting program Mosfit. The isomer shift values are quoted relative to that of α-Fe at 300 K.

3. Results and discussion

3.1. Study of the as-prepared oxygen passivated nancrystalline iron

Fig. 1a shows a TEM micrograph of the as-prepared material (i.e., sample after inert gas evaporation and passivation with oxygen). The sample is formed by spherical grains with a high degree of coalescence or interconnection between them. A log normal particle size distribution is observed while the mean particle diameter is estimated at about 17 nm [18]. In the micrograph it is possible to identify in some particles a dark core surrounded by a clear layer indicating a core/shell structure.

The XRD analysis of the as-prepared ultrafine powders (see Fig. 5) reveals the presence of pure α-Fe and some small and very broad features at the position of the peaks for the spinel iron oxide phase (γ-Fe_2O_3 and/or Fe_3O_4). The presence of oxide species at the surface of the passivated nanocrystalline powders has been fully confirmed by XPS [19].

Fig. 1b shows the EELS spectra (O-K and Fe-$L_{2,3}$ edges) recorded from the core and from the shell of one nanoparticle. The number of oxygen atoms is similar in both spectra while the number of iron atoms is higher in the core. The shape of the Fe-$L_{2,3}$ edge corresponding to the spectrum recorded in the core is more similar to a metallic iron, while in the shell it is more similar to that of an iron oxide [24]. This new result obtained by EELS confirms a core/shell structure where the dark inner zone surrounded by a light layer correspond to metallic iron and to the oxide phase, respectively. This Fe/Fe_xO_y structure of the nanocomposite has been also visualised by EFTEM (Energy Filtered Transmission Electron Microscopy) [25].

The selected area electron diffraction pattern depicted in Fig. 2a, shows the presence of spots, due to metallic α-Fe, and diffuse rings, corresponding to the lattice spacing of cubic iron oxide (γ-Fe_2O_3 and/or Fe_3O_4). The oxide phase may crystallize partially under the electron beam [26]: in this sense, it has been included in Fig. 2b a high resolution TEM image of the sample, where the core-shell structure is clearly observed, and where small crystals of γ-Fe_2O_3/Fe_3O_4 with size of about 2–3 nm have been identified.

However, none of the techniques above described allow to determine which of the two spinel phases constitute the oxide layer, and none of them can provide a quantitative estimation of the metal/oxide ratio in the sample. Other techniques are needed at this point in order to get a fully microstructural characterization of the as-prepared material. The XANES (X-ray Absorption Near Edge Structure) region of the XAS spectra contains information about oxidation states and local structure around the absorbing atom. Although multiple scattering calculations can be carried out to simulate the XANES spectra, also a fingerprint technique can be used to obtain conclusions from these data, only by comparison with reference samples [27]. Thus, we have plotted in Fig. 3a the spectrum at the Fe-K edge for the as prepared sample together with the spectra for a metallic Fe foil and γ-Fe_2O_3 and Fe_3O_4 references samples. It is clear that the spectrum corresponding to

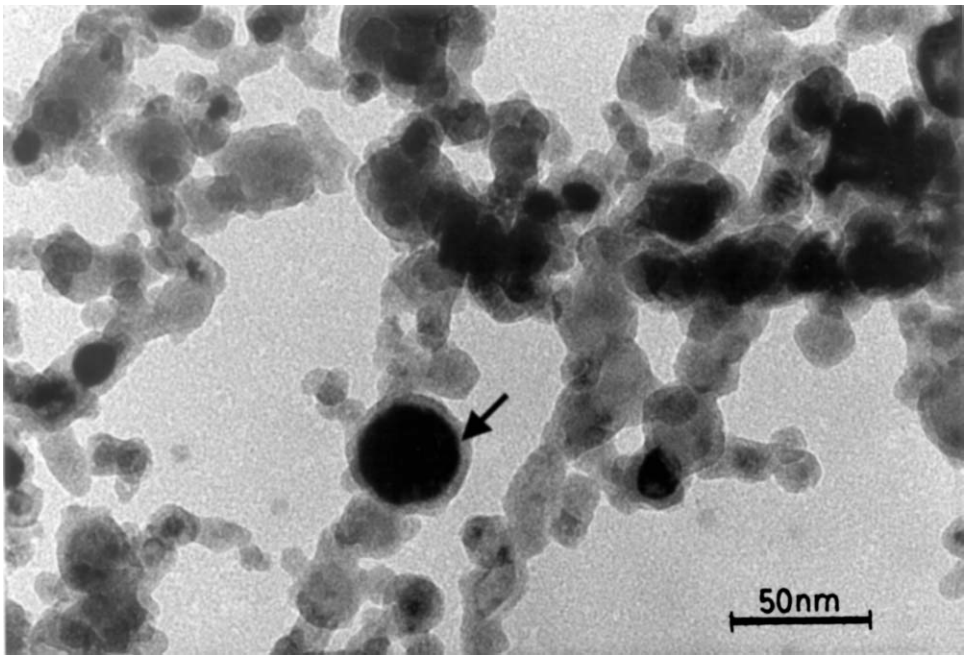

(a)

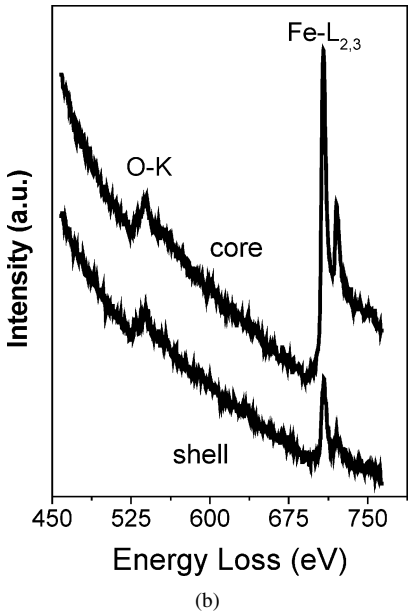

(b)

Figure 1 (a) TEM bright field micrograph of the Fe/Fe_xO_y as-prepared sample. (b) EELS spectra at the O-K edge and Fe-K edge measured in the core and in the shell of the nanoparticle marked in the TEM image.

the sample presents a higher intensity of the features at 7113 eV and a decrease in the intensity of the white line at 7132 eV in comparison to the oxides. This also seems to indicate that the as-prepared sample results from a mixture of metallic iron and iron oxide. Due to the metallic iron content it is not easy to identify the spinel oxide which constitutes the surrounding shell.

To estimate the oxide to metal ratio, linear combinations of the reference spectra for Fe^0 and γ-Fe_2O_3 have been carried out to achieve the best reproduction of the experimental spectrum for the sample. This linear combination is represented in Fig. 3b giving a quantification of the bulk composition of the oxide-metal nanocomposite material. The best fit is found for a composition of 28% of metallic iron. It should be considered here that better reproduction of the experimental spectrum should be obtained if we could use a reference spectra for amorphous "Fe_2O_3" instead of that characteristic of a γ-Fe_2O_3 microcrystalline sample. At that point we may also consider that similar results can be obtained using the spectrum of Fe_3O_4 as one component.

Because none of the analytical and spectroscopic techniques have been able to unambiguously identify the oxide phase present in the sample, the sample was studied by ^{57}Fe Mössbauer spectrometry. Indeed, this technique is suitable to evidence for the valence state of iron atoms present in the sample, the paramagnetic or magnetically ordered state of iron-based phases, and the presence of superparamagnetic effects, if any, whatever the atomic structure is. Let us also emphasize that the hyperfine structures of bulk iron oxides are quite different and the values of the hyperfine parameters allow the phase to be identified. Nevertheless the situation is much more complex in presence of structural

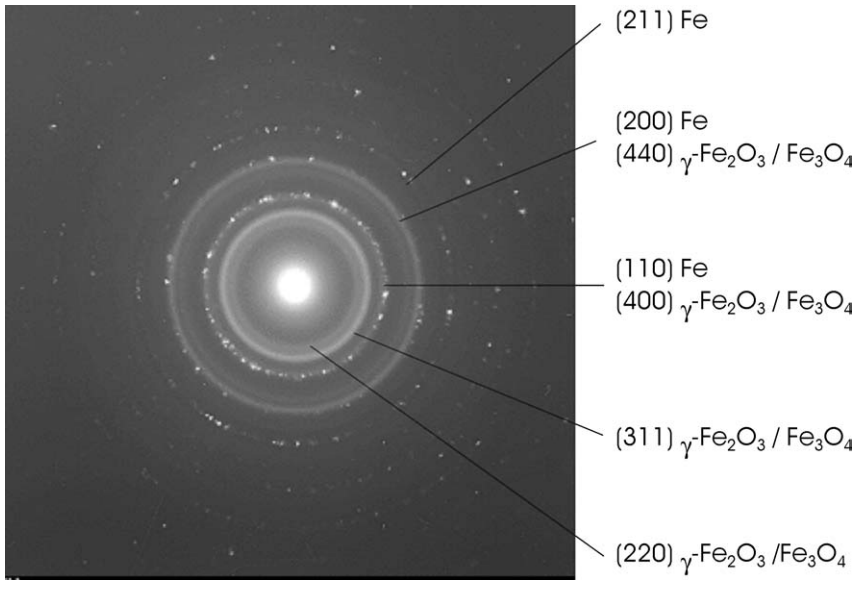

(a)

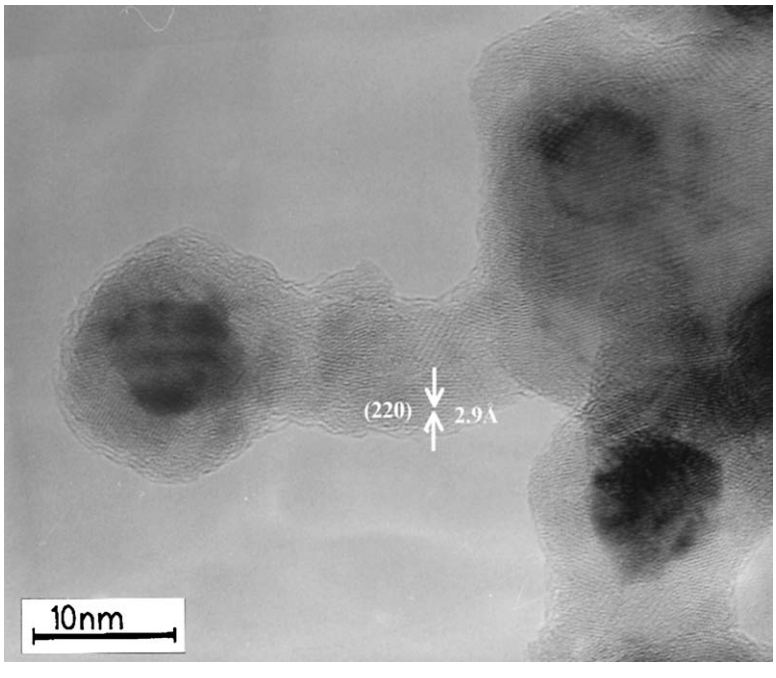

(b)

Figure 2 (a) Indexed electron diffraction pattern from the as prepared Fe/Fe$_x$O$_y$ sample. (b) High resolution TEM image.

disorder, defect, vacancies, lack of stoichiometry and confinement into grains or nanoparticles.

Fig. 4 shows the zero-field Mössbauer spectra at 77 and 4.2 K and a 6 T field spectrum at 10 K, recorded on the as-prepared sample. The spectra are composed of two main magnetic components; the first component (dashed line), with rather well defined lines, is unambiguously assigned to the α-Fe, while the second component (dot line), with asymmetrical and broad lines, can be fitted by means of a discrete distribution of hyperfine fields. It is also observed that the broadening of the lines decreased when the temperature decreases. The mean values obtained for the hyperfine field, B_{hyp} and the isomer shift, IS, are listed in Table I. The second component is thus assigned to the presence of high spin state Fe^{3+} ions, consistent with the Fe oxide phase. Assuming the same recoilless factors, the relative area of the metallic iron component is estimated at about 25% of total iron, that is in good agreement with data obtained by XAS.

It is important to emphasize that the Mössbauer spectra do not present any quadrupolar component at both

TABLE I Hyperfine characteristics deduced from zero-field Mössbauer spectrum on the as-prepared sample. (IS is the isomer shift quoted relative to metallic Fe at 300 K, 2ε the quadrupolar shift, B_{hyp} the hyperfine field.)

	$\langle$IS$\rangle$ (mm/s) $\pm.02$	$\langle 2\varepsilon \rangle$ (mm/s) $\pm.02$	$\langle B_{\text{hyp}} \rangle$ (T) ± 0.5	(%) ± 2
77 K				
α-Fe	0.12	0.01	34.2	27
Fe oxide	0.47	−0.01	47.0	73
4.2 K				
α-Fe	0.13	0.03	34.5	24
Fe-oxide	0.47	0.00	50.0	76

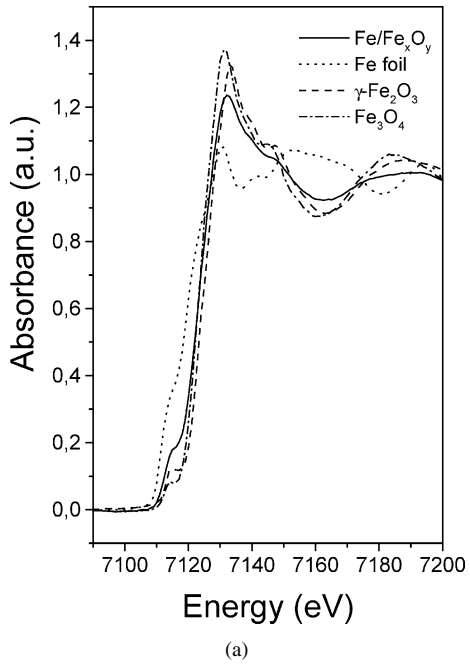

(a)

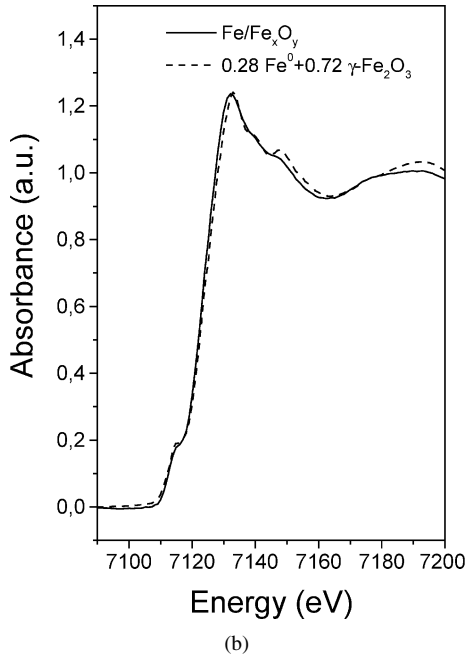

(b)

Figure 3 (a) XAS spectra at the Fe K edge for the Fe/Fe_xO_y sample in comparison to a metallic Fe foil, γ-Fe_2O_3 and Fe_3O_4 reference samples. (b) The spectrum for the nanocrystalline composite sample (full line) is compared with the linear combination (dashed line) of the spectra for Fe and γ-Fe_2O_3.

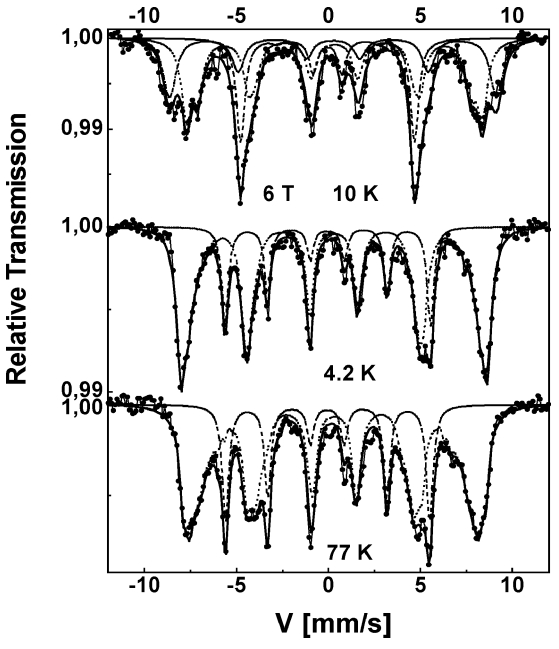

Figure 4 Mössbauer spectra registered in the as-prepared sample under zero applied field at 77 K and 4.2 K and at 10 K under an applied magnetic field of 6 T.

77 and 300 K: this indicates that the ferric component is not amorphous, but presents a long-range crystalline order. Indeed, the freezing temperature of amorphous oxides is usually ranged within the range 30–60 K. It is also useful to note that although the oxide crystallites should be smaller than 5 nm, no central superparamagnetic absorption is observed in the spectrum at 77 K. Indeed, it is expected that non interacting γ-Fe_2O_3 nanoparticles with diameters below 5 nm have superparamagnetic blocking temperature below 80 K [28]. This different behaviour can be explained due to the interaction between adjacent iron oxide and iron metallic nanocrystallites [29]. Finally, no significant divalent iron phase can be identified from the hyperfine structure, neither at 77 K nor at 4.2 K. This feature is not in favour of the presence of magnetite which exhibits a clearly localized Fe^{2+} site below the Verwey transition, in the bulk state.

One observes on the spectrum recorded at 10 K under an external magnetic field of 6 T applied parallel to the γ-beam (Fig. 4c) a sizeable increase of the intermediate lines and two asymmetrical outer lines. This is *a priori* characteristic of an alignment of iron magnetic moments, perpendicular to the γ-radiation, i.e., to the external magnetic field. The spectrum has been thus decomposed into three magnetic sextets. According to the isomer shift value, one sextet is unambiguously assigned to the metallic phase. In addition, its effective field (equivalent to the vectorial sum of the hyperfine field at Fe nucleus and the external magnetic field) is estimated at 29.1 T: indeed, it is well established that the Fermi term which is negative, leads to an hyperfine field opposite to its magnetic moment. Under the applied field, the iron moment is oriented parallel to the external field favoring thus a lowering of the effective field and a considerable decrease of the intensities of intermediate lines, as observed here. The relative area of the α-iron component is again found to be 25%, in agreement with the value previously found under zero applied field, and with the value obtained by XANES spectroscopy.

The remaining component assigned to the oxide phase has been fitted with two broad lines sextets (see Table II) with mean effective fields of 55.2 and 48.2 T, and an isomer shift of 0.42 and 0.52 mm/s. These values are the expected ones respectively for octahedral and tetrahedral iron sites and the differences as well (typically of about 0.11 mm/s), what enables to rule out the presence of α-Fe_2O_3. The isomer shift values of both octahedral and tetrahedral iron sites, are in good agreement with the expected values for the

TABLE II Hyperfine characteristics deduced from zero-field and under field Mösbauer spectra on the as-prepared sample. (IS is the isomer shift quoted relative to metallic Fe at 300 K, 2ε the quadrupolar shift, B_{hyp} the hyperfine field (zero applied field), B_{eff} the effective field (under magnetic field) at iron sites and θ the angle defined between the direction of Fe moments and the γ-beam).

	⟨IS⟩ (mm/s) ±.02	⟨2ε⟩ (mm/s) ±.02	⟨B_{eff}⟩ (T) ±0.5	⟨θ⟩ (○) ±5	⟨B_{hyp}⟩ (T) ±0.5	(%) ±2
4.2 K						
α-Fe	0.13	0.03	–	–	34.5	24
Fe oxide	0.47	0.00	–	–	50.0	76
10 K 6T						
α-Fe	0.14	0.00	29.1	11	34.9	23
γ-Fe_2O_3 T	0.42	0.00	55.2	44	51.1	24
O	0.51	0.00	48.2	53	52.0	53

γ-Fe_2O_3, what enables to determine the nature of the oxide phase formed in the oxide passivation layer. The ratio of the number of tetrahedral/octahedral iron sites (0.45) is rather low compared to expected one (0.60), that suggests the presence of numerous structural defects, i.e., a poor crystalline state.

In a collinear magnetic system the atomic moments lie along the direction of the external magnetic field, and the second and fifth lines of the Mössbauer spectrum will then disappear (intensity = 0). In the spectrum corresponding to this sample it is observed a high decrease of the lines 2 and 5 for the metallic iron component but not for the second component. It thus excludes that this second component behaves as a ferrimagnet but it can be explained as a consequence of a large deviation from the spin collinearity existing in the iron oxide crystallites [29, 30]. The θ values (where θ represent the angle defined by the γ-radiation and the effective field) obtained in the fitting for the components corresponding to Fe^{3+} for octahedral and tetrahedral sites are 44° and 55° respectively: this clearly indicates that the magnetic moments are strongly canted. In the case of the metallic iron this canting is only of 11°. The presence of canted spins is due to the low crystalline order in the oxide layer, and/or to interface or surface effects, that produce broken exchange bonds between spins [30].

In addition, one can calculate the hyperfine field values which are given by the expression [31]:

$$B_{hyp}^2 = B_{eff}^2 + B_{app}^2 - 2B_{eff}B_{app}\cos\theta$$

where B_{app} is the external field, B_{eff} is the effective field estimated from in-field Mössbauer spectra. The result of this calculation is included in Table II. The values obtained for B_{hyp} are in good agreement with the expected values for the metallic iron (34.5 T) and for the γ-Fe_2O_3 phase (52 y 53 T).

In this sense, and from a magnetic point of view, we can consider the nanoparticles as formed by a core-shell structure, where the magnetic moments are aligned with the field in the core and are canted at the surface. For the metallic phase, we expect a saturated core and a layer, corresponding to the interface metal-oxide, where the magnetic canting is located. We can consider a proportion of "q" moments located at the interface and "$1-q$" located in the core. The normalized amplitude of the 2 and 5 lines ($A_{2,5}$) of the Mössbauer spectrum are given by the expression:

$$A_{2,5} = 1/2\sin^2\theta = 1/2[(1-q)\sin^2\theta_c + q\sin^2\theta_l],$$
$$\text{with } q = 1-(1-e/r)$$

where θ_c and θ_l are the θ value for the core and for the layer, respectively, "e" is the thickness of the interface layer and "r" is the metallic core radius. The value of θ_c is zero, and the value of θ_l is 54.7°, corresponding to a random distribution of the moments. The obtained value for θ is 11° and we can consider $r \cong 5$ nm (from TEM measurements), with these values we obtained a value of 0.1 nm for the thickness of the metal-oxide interface at the metallic core side, so there is not an important influence of the oxide phase on the magnetic behavior of the metallic phase.

In the same way, the oxide shell can be divided into a core saturated and a surface canted layer. The θ values is about 45°, so we obtain a value of 5 nm for the thickness of the canted surface, what indicates that the total oxide layer is "non-collinear" with the field. This aspect is compatible and corroborates the spin-glass like magnetic behaviour of the oxide layer, previously evidenced and reported for this sample, where a freezing temperature $T_f = 50$ K was found [12].

The canted spins arising from reduced coordination and broken exchange bonds between surface spins was also observed by Kodama and co-workers at the surface of ferrite nanoparticles [32]. The Mössbauer technique has therefore allowed us to fully characterize, not only structurally but also magnetically, the as-prepared Fe/Fe_xO_y material.

3.2. Study of the thermal evolution in vacuum of the oxygen passivated nanocrystalline iron

Fig. 5 shows the XRD diffraction pattern of the original passivated nanocrystalline iron (as-prepared sample) and the material after heating at different temperatures under different controlled residual vacuum pressures. It is clear from this figure that the thermal treatment produces the formation of γ-Fe_2O_3 and/or Fe_3O_4. These two phases are not easily distinguish by XRD due to the similarity of the cubic lattice parameters. The sample heated at 573 K and 10^{-4} torr, is the only one that does not present any peak due to metallic iron. The sample was totally transformed to iron oxide. The peaks are broad as corresponds to nanocrystalline samples. Evaluation of the coherent domain of diffraction by the Scherrer's method, calculated for the two phases after the different thermal treatments are shown in Table III. It is obtained a value of 8.6 nm for the nanocrystallite size of the oxide sample formed during heating at 573 K under 10^{-4} torr residual vacuum pressure.

After a long period of air exposition this last sample stay unaltered, while in the others the remained iron evolves to α-Fe_2O_3, as it has been demonstrated by XRD.

A TEM general view of the sample heated at 573 K and 10^{-4} torr residual vacuum pressure is displayed

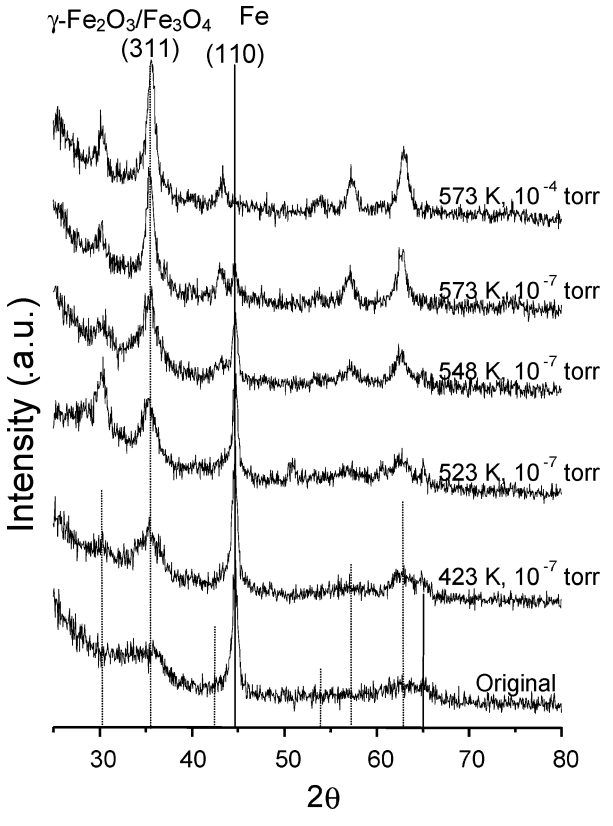

Figure 5 XRD spectrum of the as prepared sample and after the different thermal treatments indicated in the figure (temperature and residual vacuum).

in Fig. 6, showing the nanocrystalline character of the material. After the thermal treatment and conversion to the γ-Fe_2O_3/Fe_3O_4 phase, the particles appear highly interconnected with a mean particle size of ca. 25 nm. This particle size value may be different from the size of the coherent domain of diffraction (8.6 nm) as determined by XRD.

TABLE III Crystallite size for the metal and oxide phases, as obtained from the XRD diffraction lines, during thermal evolution of the Fe/Fe_xO_y sample

Sample	D (Fe_xO_y) (nm)	D (Fe) (nm)
As-prepared	–	13.6
423 K, 10^{-7} torr	4.1	13.6
523 K, 10^{-7} torr	6.5	14.9
548 K, 10^{-7} torr	10.0	13.8
573 K, 10^{-7} torr	9.4	17.0
573 K, 10^{-4} torr	8.6	–

It may also be mentioned that for this sample some particles show in the centre a clear and small inner core in the opposite way to that observed in the as-prepared sample. The formation of this structure can be explained taking into consideration the mechanism for the oxidation of metals. According to the Cabrera-Mott mechanism [33], the oxidation of metals progress by the transport of cations through the forming oxide layer. It is thus expected the migration of iron from the centre of the particle to the surface during oxidation, this may produce a lower density of material in the centre.

The EXAFS spectrum of the sample heated at 573 K and 10^{-4} torr residual vacuum pressure, has been recorded in comparison to the spectra for the two oxide spinel reference phases. In Fig. 7 are depicted the Fourier transform functions of the EXAFS oscillations at the Fe-K edge. Just by comparison of the radial distribution functions without any fitting it can be observed how the procedure described in the present work produces mainly nanocrystalline γ-Fe_2O_3 particles as stated from the position of the peaks in the radial distribution function. In this context, it is relevant to mention that the brown colour of the heated sample is characteristic of the γ-Fe_2O_3.

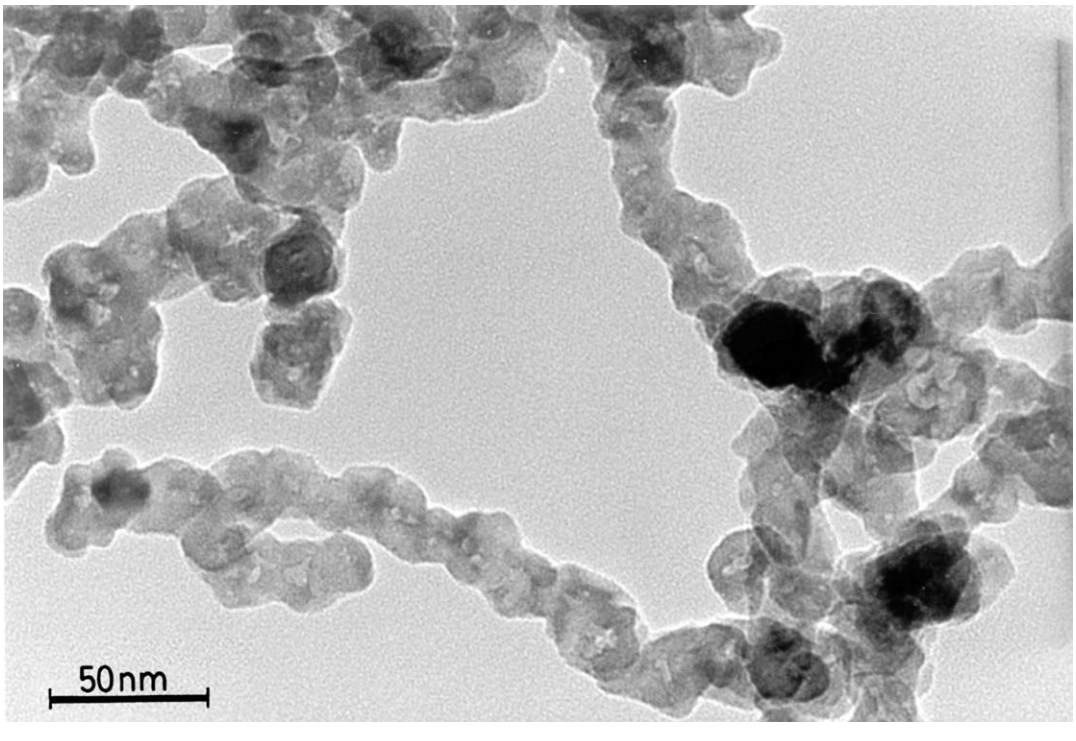

Figure 6 TEM bright field micrograph for the sample heated at 773 K in a vacuum of 10^{-4} torr.

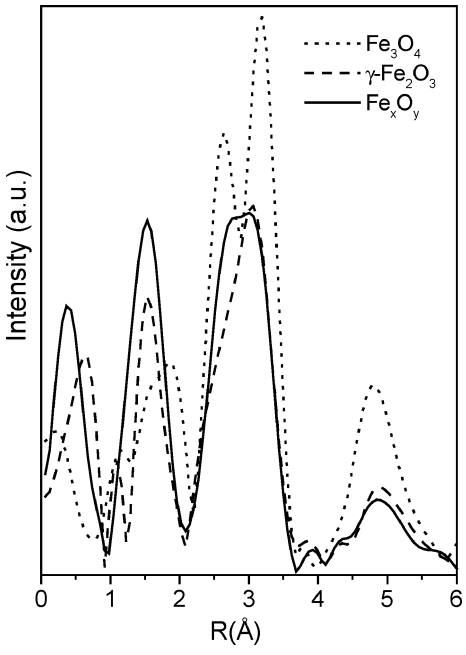

Figure 7 Experimental Fourier transforms (not corrected for the phase shift) obtained for the sample heated at 773 K in a vacuum of 10^{-4} torr in comparison to the two spinel iron oxides reference samples.

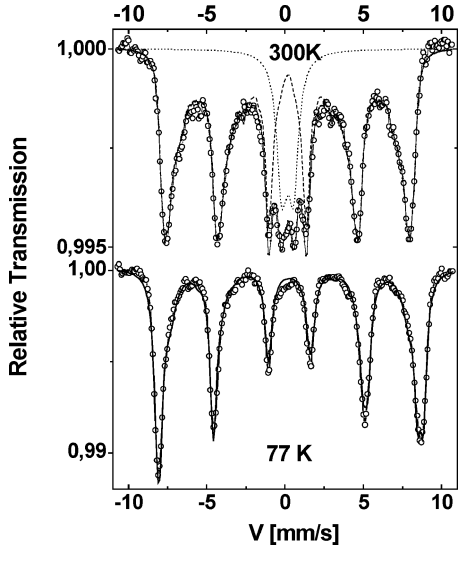

Figure 8 Mössbauer spectra registered at 77 K, and 300 K for the sample heated at 773 K in a vacuum of 10^{-4} torr.

The Mössbauer spectra registered at 77 and 300 K, corresponding to the heated sample at 4×10^{-4} torr residual vacuum pressure are represented in Fig. 8. The spectrum at 77 K is well fitted with only one component, by means of a distribution of hyperfine fields. The mean values obtained for B_{hyp} and IS are 50.2 T and 0.45 mm/s respectively (Table IV). These values are in agreement with the total transformation of the metallic iron phase to the γ-Fe_2O_3 oxide phase. In the spectrum at room temperature, it appears a quadrupolar doublet at the centre and a sextet with lines which are more broadened than those observed at 77 K. This spectrum can be thus interpreted as resulting from a wide distribution of particles size, where the smaller ones are superparamagnetic and the bigger ones (more than about 10 nm crystallite size) are completely magnetically blocked at room temperature.

TABLE IV Hyperfine characteristics deduced from zero-field Mössbauer spectra on the sample heated at 573 K under a residual pressure of 10^{-4} torr. (IS is the isomer shift quoted relative to metallic Fe at 300 K, and B_{hyp} the hyperfine field.)

Sample heated at 573 K and 10^{-4} torr	$\langle$IS$\rangle$ (mm/s) $\pm.02$	$\langle B_{\text{hype}}\rangle$ (T) ±0.5
77 K	0.45	50.2
300 K	0.36	33.7[a]

[a]Two contributions are distinguished: a doublet $\langle QS\rangle = .66$ mm/s, 16% and a sextet $\langle B\rangle = 40$ T, 84%. QS is the quadrupolar contribution.

It is important to mention that the inert gas evaporation method allows also a certain control of the particle size distribution [34], so that it will be also possible to obtain samples with controlled size of the γ-Fe_2O_3 nanocrystalline phase.

4. Conclusions

The inert gas evaporation method allowed us to prepare nanocrystalline particles formed by a metallic crystalline iron core surrounded by a shell of very small nanocrystallites of γ-Fe_2O_3. The high surface disorder of this layer and the effects at the Fe/γ-Fe_2O_3 interface produce a spin canting of the magnetic moments of the oxide layer. The singular magnetic behaviour of the as-prepared sample (exchange anisotropy [12], spin glass [12] and spin canting of the oxide layer) is well understood thanks to the complete microstructural characterization of the material.

The heating of the original passivated sample at 573 K and 4×10^{-4} torr of residual vacuum pressure, produces the almost total conversion of the material to γ-Fe_2O_3 that behaves mainly like superparamagnetic nanoparticles. The method can be proposed as a route of preparation of superparamagnetic γ-Fe_2O_3 nanomaterials.

Acknowledgements

Authors thank the DGES for financial support (Project nr.: PB96-0863-C02-02 and the Picasso Hispano-French Program: Acción Integrada HF1998-0211). The synchrotron LURE and the Materials Science Department of the Univ. of Oxford (M. J. Sayagués) are acknowledged for providing the XAS and HRTEM facilities respectively. EC COST Action 523 "Nanostructured Materials" is also thankful.

References

1. E. MATIJEVIC, *MRS Bull.* **XIV** (1989) 19.
2. Y. YOSHIZAWA, S. OGUMA and K. YAMAUCHI, *J. Appl. Phys.* **64** (1988) 6044.
3. E. F. KNELLER and R. HAWIG, *IEEE Trans. Magn.* **MAG-27** (1991) 3588.
4. S. W. CHARLES, in "Magnetic Properties of Fine Particles" edited by J. L. Dormann and D. Fiorani (Elsevier, Amsterdan, 1991) p. 2676.
5. W. WAGNER, H. VAN SWYGENHOVEN, H. J. HÖFLER and A. WIEDENMANN, *Nanostruct. Mater.* **6** (1995) 929.
6. W. GONG, H. LI, Z. ZHAO and J. CHEN, *J. Appl. Phys.* **69** (1991) 5119.

7. S. GANGOPADHYAY, G. C. HADJIPANAYIS, S. I. SHAH, C. M. SORENSEN, K. J. KLABUNDE, V. PAPAEFTHYMIOU and A. KOSTIKAS, *ibid.* **70** (1991) 5888.
8. J. LÖFFLER, H. VAN SWYGENHOVEN, W. WAGNER, J. MEIER, B. DOUDIN and J. PH. ANSERMET, *Nanostruct. Mater.* **9** (1997) 523.
9. H. KISKER, T. GESSMANN, R. WÜRSCHUM, H. KRONMÜLLER and H. E. SCHAEFER, *ibid.* **6** (1995) 925.
10. S. GANGOPADHYAY, G. C. HADJIPANAYIS, B. DALE, C. M. SORENSEN and K. J. KLABUNDE, *ibid.* **1** (1992) 77.
11. W. H. MEIKLEJOHN and C. P. BEAN, *Phys. Rev.* **105** (1957) 904.
12. L. DEL BIANCO, A. HERNANDO, M. MULTIGNER, C. PRADOS, J. C. SÁNCHEZ-LÓPEZ, A. FERNÁNDEZ, C. F. CONDE and A. CONDE, *J. Appl. Phys.* **84** (1998) 2189.
13. S. GANGOPADHYAY, G. C. HADJIPANAYIS, B. DALE, C. M. SORENSEN, K. J. KLABUNDE, V. PAPAEFTHYMIOU and A. KOSTIKAS, *Phys. Rev.* B **45** (1992) 9778.
14. L DEL BIANCO, D. FIORANI, A. M. TESTA, E. BONETTI, L. SAVINI and S. SIGNORETTI, *Phys Rev* B **66** (2002) 174418.
15. T. UCHIKOSHI, Y. SAKKA, YOSHITAKE and K. YOSHIHARA, *Nanostruct. Mater.* **4** (1994) 199.
16. J. LÖFFLER, W. WAGNER, H. VAN SWYGENHOVEN and A. WIEDENMANN, *ibid.* **9** (1997) 331.
17. L. THEIL KUHN, A. BOJESEN, L. TIMMERMANN, M. MEEDOM NIELSEN and S. MORUP, *J. Phys.: Condens. Matter* **14** (2002) 13551.
18. J. C. SÁNCHEZ-LÓPEZ, A. JUSTO, A. FERNÁNDEZ, C. F. CONDE and A. CONDE, *Philos. Mag.* B **76** (1997) 663.
19. J. C. SÁNCHEZ-LÓPEZ and A. FERNANDEZ, *Mater Sci Forum* **269–272** (1998) 827.
20. C. PRADOS, M. MULTIGNER, A. HERNANDO, J. C. SANCHEZ-LOPEZ, A. FERNANDEZ, C. F. CONDE and A. CONDE, *J. Appl. Phys.* **85** (1999) 6118.
21. B. MARTINEZ, A. ROIH, X. OBRADORS, E. MOLINS, A. ROUANET and C. MONTY, *ibid.* **79**(5) (1996) 2580.
22. S. MORUP and S. LINDEROTH, in "Nanophase Materials, NATO ASI Series E: Applied Sciences," edited by G. C. Hadjipanayis and R. W. Siegel (Dordrecht, Kluwer, 1994) Vol. 260 p. 595.
23. H. GLEIDER, *Avd. Mater.* **4** (1992) 479.
24. L. A. GRUNES, *Phys. Rev. B* **27**(4) (1983) 2111.
25. M. J. SAYAGUÉS, T. C. ROJAS, A. FERNÁNDEZ, R. E. DUNIN-BORKOWSKY, R. C. DOOLE and J. L. HUTCHISON, *Microscopy and Microanalysis* **8** (2002) 403.
26. T. C. ROJAS, J. C. SÁNCHEZ-LÓPEZ, M. J. SAYAGUÉS, E. P. REDDY, A. CABALLERO and A. FERNÁNDEZ, *J. Mater. Chem.* **9** (1999) 1011.
27. A. BIANCONI, in "X-ray Absorption: Principles, Applications, Techniques of EXAFS, SEXAFS and XANES," edited by D. C. Konigsberger and R. Prins (John Wiley, New York, 1988) Chap. 11, p. 573.
28. E. TRONC, P. PRENE, J. P. JOLIVET, F. DÓRAZIO, F. LUCARI, D. FIORANI, M. GODINHO, R. CHEKAOUI, M. NOGUES and J. L. DORMANN, *Hyper. Interact.* **95** (1995) 129.
29. H. HANEDA and A. H. MORRISH, *Surf. Sci.* **77** (1978) 584.
30. A. H. MORRISH and K. HANEDA, *J. Magn. Magn. Mater.* **35** (1983) 105.
31. N. RANDRIANANTOANDRO, P. LAFFEZ, C. SELLA and J. M. GRENECHE, *Eur. J. Phys.: Appl. Phys.* **9** (2000) 125.
32. R. H. KODAMA, A. E. BERKOWITZ, E. J. MC. NIFF and S. FONER , *J. Appl. Phys.* **81** (1977) 5552.
33. N. CABRERA and N. F. MOTT, *Rep. Prog. Phys.* **12** (1949) 163.
34. J. C. SÁNCHEZ-LÓPEZ, A. JUSTO and A. FERNÁNDEZ, *Langmuir* **15** (1999) 7822.

Received 22 January 2003
and accepted 27 April 2004